Applied Physics Letters

RESEARCH ARTICLE | OCTOBER 21 2024

Using an electrically charged mist to visualize the potential wells in "sonomaglev," a combined diamagnetic-acoustic levitator

George Hunter-Brown; Naresh Sampara; Matthew M. Scase; Richard J. A. Hill

Appl. Phys. Lett. 125, 174101 (2024)
https://doi.org/10.1063/5.0226729

Applied Physics Letters ARTICLE pubs.aip.org/aip/apl

Using an electrically charged mist to visualize the potential wells in "sonomaglev," a combined diamagnetic-acoustic levitator

Cite as: Appl. Phys. Lett. **125**, 174101 (2024); doi: 10.1063/5.0226729
Submitted: 3 July 2024 · Accepted: 9 October 2024 ·
Published Online: 21 October 2024

View Online Export Citation CrossMark

George Hunter-Brown,[1] Naresh Sampara,[1] Matthew M. Scase,[2] and Richard J. A. Hill[1,a)]

AFFILIATIONS

[1]School of Physics and Astronomy, University of Nottingham, Nottingham NG7 2RD, United Kingdom
[2]School of Mathematical Sciences, University of Nottingham, Nottingham NG7 2RD, United Kingdom

[a)]Author to whom correspondence should be addressed: richard.hill@nottingham.ac.uk

ABSTRACT

We use a water mist to experimentally visualize the wells in the potential energy of material levitated by a combined diamagnetic-acoustic levitator. The levitator consists of an 18.5 T superconducting magnet, which can levitate diamagnetic material, such as water, plastics, and organic materials, by applying a magnetic body force counteracting the force of gravity. Low-power ultrasound transducers operated at 37.5 kHz generate an acoustic field that spatially modulates the net force acting on the diamagnetically levitated material, making "sonomaglev" capable of levitating multiple objects in stable equilibrium. In these experiments, we levitate a mist of water droplets that are electrically charged so that they repel each other, preventing them from coalescing as a single drop in each of the local potential minima. The shapes of the potential wells are revealed by the shapes of clusters of droplets, which conform to the isosurfaces of the sum of the magnetic, gravitational, and acoustic potentials. The spacing of the droplets in a cluster is shown to depend on their charge, volume, and the force constant of the well in a simple model. Compared to acoustic levitation alone, the combination of diamagnetic and acoustic levitation allows more scope for the manipulation of levitated objects, since the acoustic field is not constrained by the requirement to balance the force of gravity. The method demonstrated here allows the influence on the potential energy of switching on the acoustic field to be observed directly.

Recently, we demonstrated sonomaglev, an experimental method combining techniques from both acoustic and diamagnetic levitation for contactless manipulation of water drops in an environment mimicking "zero-G," in the laboratory.[1] The method can also be readily extended to other diamagnetic material such as organic liquids, plastics, and biological material. Diamagnetic levitation uses a strong, spatially varying magnetic field to exert a force on a diamagnetic object that exactly balances the object's weight.[2–4] This magnetic force is a body force as it acts throughout the object, at the molecular level. A field of intensity $B \sim 10\,\mathrm{T}$ is typically required to levitate such materials, though suspension in weaker magnetic fields can also be achieved if the object is immersed in a paramagnetic fluid, by exploiting the magneto-Archimedes effect.[5–7] In acoustic levitation, high-frequency (20–100 kHz) sound waves are used to exert acoustic radiation forces on objects to suspend them against the force of gravity.[8,9] Acoustic levitation has found numerous applications, in part due to the ability to generate a field of force that can manipulate the position and orientation of single and multiple objects (see, e.g., Refs. 10–13). The acoustic levitation method does have some undesirable characteristics, however, originating from the fact that the acoustic forces suspending the object are time-varying and act at the surface of the object. Acoustically levitated material has a tendency to oscillate and rotate;[14,15] liquid drops tend to be deformed into oblate-like shapes and become increasingly more deformed with increasing ratio of the diameter to the acoustic wavelength; the time-varying acoustic pressure generates streaming flows in the air, which also set up flows within the drop, affecting heat and mass transfer at the surface.[14,16] By combining the two methods, we can retain the desirable characteristics of acoustic levitation—its ability to readily manipulate objects via acoustic forces—without such drawbacks, since the sound pressure level of the acoustic field is much reduced, by a factor ~ 100, compared to that of a typical acoustic levitator.[1] Since the acoustic forces are not required to balance the force of gravity, there is also more freedom to use the acoustic field to manipulate the objects, while maintaining the levitation.

To fully exploit sonomaglev for manipulating objects in three-dimensions, we require the ability to predict the forces on the levitated objects. A variety of techniques may be used to model the pressure fields produced by the acoustic transducers, including far-field approximations,[17] matrix methods for reflections,[18,19] finite element methods,[1,19] and boundary element methods.[20] The magnetic forces can be calculated from the magnetic field profile of the magnet, which can be computed from the solenoid geometry, if known, and the magnetic mass susceptibility of the material. Experimentally, it is possible to measure the acoustic field using microphones,[18] but to map a three-dimensional volume using this technique can be time-consuming, and reflections from the microphone can influence the acoustic field being measured. Optical techniques such as schlieren,[21,22] shadowgraphy,[21,22] synthetic schlieren,[22,23] and optical feedback interferometry[24] allow for the visualization of acoustic fields without disturbing the underlying acoustic field. Experimental measurements of the magnetic field can be made using a Hall-effect sensor.

Here, we take the approach of experimentally measuring the shapes of the potential wells in the combined magnetic, gravitational, and acoustic potential energy of levitated test particles directly. This method can be regarded as similar to Kundt's well-known experiment[25,26] to measure the wavelength of sound. In Kundt's tube experiment, a fine dust of small particles is subjected to sound waves generated at one end of the tube, which collect at the nodes in the pressure wave. Rather than dust particles, the test particles used in these experiments are small, electrically charged water droplets that are freely suspended in stable equilibrium diamagnetically, before the imposition of the acoustic field. The charge causes the droplets to repel one another, which would otherwise coalesce into a single drop at each of the potential minima.[1]

The potential energy densities associated with the external forces acting on the droplets, the gravitational (g), magnetic (m), and acoustic (a) forces, are given by $u_g = (D_{wat} - D_{air})gz$, $u_m = (\chi_{air} - \chi_{wat})B^2/(2\mu_0)$, and $u_a \approx \frac{1}{2}\langle p^2\rangle/(D_{air}c_{air}^2) - \frac{3}{4}D_{air}\langle v^2\rangle$ in this case.[1,27,28] Here, $\chi_{wat} = -9.05 \times 10^{-6}$, $\chi_{air} = 5.13 \times 10^{-7}$, $D_{wat} = 998\text{kgm}^{-3}$, and $D_{air} = 1.2\text{kgm}^{-3}$ are the volume magnetic susceptibilities (S.I.) and densities, respectively, at room temperature,[29–31] $c_{air} = 343\text{ms}^{-1}$ is the speed of sound in air, B is the magnetic induction intensity, g is the acceleration due to gravity, μ_0 is the vacuum permeability, z is the vertical coordinate, and $\langle p^2\rangle$ and $\langle v^2\rangle$ are the mean square fluctuations in time of the pressure and velocity fields, respectively. The net external force acting on a droplet is $\mathbf{F} = -\mathscr{V}\nabla u$, where $u = u_g + u_m + u_a$ and $\mathscr{V}$ is the droplet's volume. The stable levitation points correspond to locations where there is a local minimum in u.

The set-up used here is similar to that described in Ref. 1. It consists of a custom-built 18.5 T superconducting magnet manufactured by Cryogenic Ltd., London. The magnet has a room temperature 58 mm diameter vertical bore, open at both ends. In the absence of acoustic forces, there exists a single stable levitation point for water when the solenoid current I lies within a narrow range,[3] which, for this magnet, produces a field at the center of the solenoid with magnetic induction intensity $B_0(I) \approx 17$ T. The stable levitation point lies on the axis of the solenoid approximately 11 cm above its center, where $B \approx 11$ T. We define a coordinate system with this point at the origin, with vertical axis z, and x and y axes in the horizontal plane. Into the bore of the magnet, we insert a 3D-printed plastic (PLA) ring with an inner diameter of 39 mm, outer diameter of 57 mm, and a height of 20 mm, containing two ultrasonic transducers (CamdenBoss CTD40K1007T), 10 mm in diameter, of the type used in the "TinyLev" acoustic levitator.[17] The transducers are positioned facing each other along the x axis, as shown in Fig. 1, and driven in-phase by a signal generator (Stanford Research DS345) at 37.5 kHz, corresponding to an acoustic wavelength $\lambda = 9$ mm and up to a maximum peak-to-peak voltage of 20 V. The transducers are not driven at their nominal resonant frequency of 40 kHz, since this produced whispering gallery modes,[32] which destabilizes the levitating droplets.[1]

A brass water mist sprayer with a 1 mm diameter nozzle was used to spray a mist of distilled water droplets, of diameter $\sim$100 μm, directly above the mouth of the magnet bore, which then descended toward the levitation point under gravity. The water pressure at the nozzle is estimated to be 2 bar. By comparison, the theoretical minimum size of water droplets that could be levitated diamagnetically in this magnet, limited by Brownian motion, is $\sim$0.1 μm diameter at room temperature. To charge the droplets, the spray bottle could be raised to a voltage 100–500 V above ground by connecting it to a current-limited ($I < 10\ \mu$A) DC power supply, though, in practice, we found that using a plastic nozzle on the spray bottle was just as effective at generating charge on the droplets. The effect of diamagnetic forces on water fog has been investigated by Lu *et al.*,[33] but in those experiments, the droplets were much smaller ($<$5 μm diameter) and uncharged. Images of the charged droplet clouds were captured using a camera sited approximately 2 m from the magnet, using a 45° mirror above the magnet to view the mist down the bore. We compared our experimental results with a numerical model. To obtain u_m, B was calculated from the known current density and geometry of the solenoid using the Biot–Savart law; u_a was calculated by a finite element method, using the open-source software FreeFEM[34] and Gmsh,[35] taking into account acoustic reflections within the magnet bore. Further details are given in Ref. 1.

A cloud of charged droplets levitated diamagnetically—without acoustic forces—is shown in Fig. 2(a). The droplets assemble around the single local minimum in the potential u, at $(x, y, z) = (0, 0, 0)$. Although electrostatic repulsion between the droplets prevents the

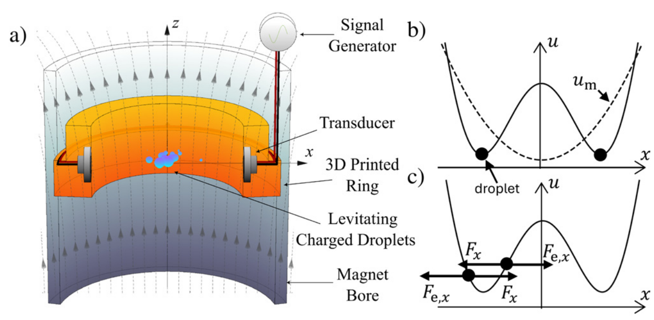

FIG. 1. (a) Diagram of the experimental set-up inside the superconducting magnet bore. The two ultrasonic transducers are aligned along an axis, x, perpendicular to the vertical bore axis, z. Dashed lines represent the magnetic field lines. Schematics illustrating the forces acting on the droplets along the x axis: (b) uncharged droplets collect at the minima in the sum of the gravitational, magnetic, and acoustic energy densities of water, u; (c) the separation between like-charged droplets is governed by the balance between the electrostatic repulsion $\mathbf{F}_e$ acting between them and the external force $\mathbf{F} = -\mathscr{V}\nabla u$ acting on them, where $\mathscr{V}$ is the droplet volume.

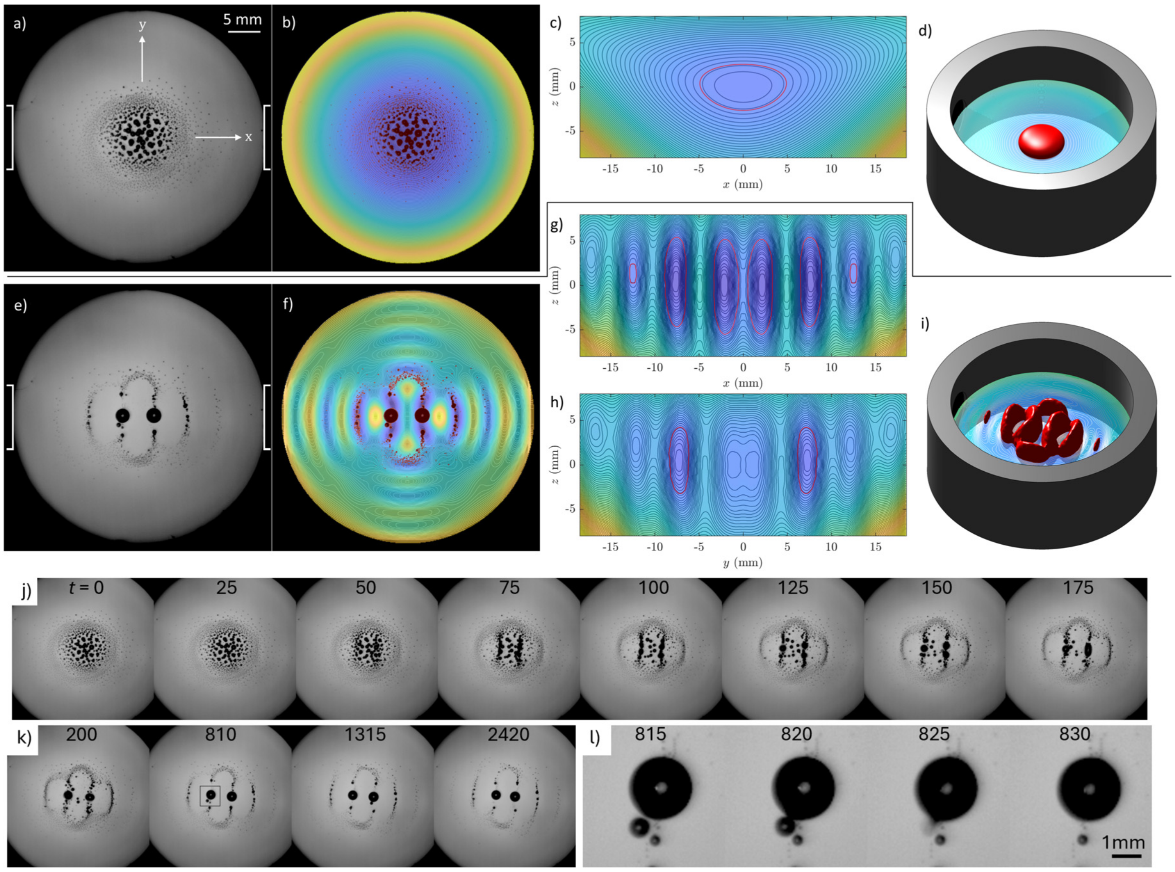

FIG. 2. (a) Image of a cloud of diamagnetically levitated, electrically charged water droplets, with no acoustic field; (b) same image superimposed on contours of u, in the horizontal $x - y$ plane at $z = 0$. White symbols mark the position of the acoustic transducers. (c) Contours of u in the $x - z$ plane at $y = 0$. In the absence of the acoustic field, u has cylindrical symmetry around the z axis. (d) Three-dimensional view of an isosurface of u corresponding to the red contour in (c); the gray ring represents the PLA ring holding the transducers, and the blue/green contours are the same as those shown in (b). (e)–(i) Same as (a)–(d), 800 ms after the ultrasound transducers were switched on; (h) shows the contours of u in the $y - z$ plane at $x = 0$. (j)–(k) Image montage showing the migration of the droplets to new equilibrium positions as the acoustic field is switched on; (j) $t = 0$–175 ms after the acoustic transducers are switched on; and (k) $t = 200$–2420 ms. The box in the $t = 810$ ms image highlights the coalescence of two drops, shown in more detail in (l). "Motion-blur" can be observed at $t = 825$ ms as the smaller droplet is absorbed into the larger.

cloud coalescing into a single drop, some coalescence between colliding droplets takes place before equilibrium is established, resulting in a cluster of larger droplets near the center of the trap. The droplet cloud attains an axisymmetric shape as expected from the cylindrical symmetry of the magnetic field. While several of the larger droplets appear to be touching or in the process of coalescing from this still image, they are, in fact, separate droplets, displaced from each other in the vertical z direction. Figure 2(b) shows the same image overlaid on contours of u in the $z = 0$ (x–y) plane. A contour plot of u in the $y = 0$ (x–z) plane is shown in Fig. 2(c). Figure 2(d) shows an isosurface of u, corresponding to the red contour in Fig. 2(c), illustrating the three-dimensional volume occupied by the droplet cloud.

Figure 2(e) shows the same charged droplet cloud as in Fig. 2(a) 800ms after the ultrasonic transducers were switched on, driven at 20 V peak-to-peak. The addition of the acoustic forces on the droplets results in their rearrangement as the system finds its new minimum energy configuration. In place of the single cylindrically symmetric potential well, the mist now reveals the presence of multiple arc-shaped potential wells along a line between the centers of the two acoustic transducers, spaced approximately $\lambda/2$ apart. Figure 2(f) shows the contours of u in the $z = 0$ (x–y) plane. Good agreement is obtained between the locations of the droplets observed experimentally and the shapes and locations of the potential wells calculated by the model, with the transducer power the only adjustable parameter in the model. The magnitude of the restoring forces in the x–y plane is of order ten times that in the vertical direction as can be seen from spacing of the contours in Figs. 2(g) and 2(h). The isosurfaces with the same potential as that in Fig. 2(d) form twisted disc-like shapes, aligned perpendicularly to the vertical z axis, as shown in Fig. 2(i). This agrees with our experimental observations, which show the droplets tightly confined at the locations of the potential wells in the x–y plane.

In the absence of acoustic forces, the cluster shown in Fig. 2 can be divided approximately into three nested layers: a diffuse outer layer of droplets with diameter $d = 260 \pm 20\ \mu$m spaced $a = 1100 \pm 100\ \mu$m apart (mean $\pm$ s.d.); a middle layer of smaller, more closely spaced droplets, $d = 150 \pm 10\ \mu$m, $a = 260 \pm 30\ \mu$m; and an inner region of much larger droplets with a wider variation in sizes, $d = 400$–$1200\,\mu$m, $a = 600$–$1000\,\mu$m resulting from the coalescence of smaller droplets. The equilibrium spacing a between droplets is governed by the balance between the electrostatic repulsion between the droplets and the externally applied force $\mathbf{F}$. Calculating the electric field inside an arbitrary-shaped cluster of charged droplets is a non-trivial problem.[36] Nevertheless, we can gain some insight into the relationship between the charge on the droplets and a by considering the simpler problem of a spherically symmetric cluster composed of layers of charged droplets in a spherically symmetric parabolic potential $u(r) = \frac{1}{2}Kr^2$. Within each layer, we assume that the droplets are equally spaced and have equal charge q_d and volume $\mathscr{V}_d$ in this model. The electric field at a distance r from the center of the spherical distribution is $E_r \approx Q(r)/4\pi\varepsilon_0 r^2$, where $Q(r)$ is the net charge enclosed within the spherical region of radius r.[37] The net force, including electrostatic forces, on a droplet in a particular layer at a distance r from the center is $F_{\mathrm{net},r} = q_d E_r(r) - \mathscr{V}_d K r$. It follows that $Q \approx 4\pi\varepsilon_0 K r^3 \mathscr{V}_d/q_d$ in equilibrium. The charge in a thin spherical shell of thickness Δr within the layer is, thus, $(\Delta Q \approx q_d \cdot 4\pi r^2 \Delta r/a^3) \approx 4 \cdot 3\pi\varepsilon_0 K r^2(\mathscr{V}_d/q_d)\Delta r$. Hence, $q_d^2 \approx 3\varepsilon_0 K a^3 \mathscr{V}_d$: the spacing between the droplets, a, within a particular layer depends only on K and the droplets' charge and volume in this model. Re-arranging this equation gives the spatially averaged charge density $\rho \approx q_d/a^3$ and volume fraction $\phi \approx \mathscr{V}_d/a^3$ in a layer in terms of K and the charge/volume ratio of the droplets $\rho_d = q_d/\mathscr{V}_d$: $\rho \approx 3\varepsilon_0 K/\rho_d$ and $\phi \approx 3\varepsilon_0 K/\rho_d^2$. Stability is governed by the total energy of the system $U_{\mathrm{tot}} = U + U_e$, where $U = 2\pi K\int_0^\infty \phi r^4 dr$ and $U_e = \frac{1}{\varepsilon_0}\int_0^\infty \rho Q r dr$,[38] from which we see that a cluster formed of droplets with constant ρ_d (constant ρ and ϕ) would be in neutral equilibrium. Using a value of $K = 5 \times 10^4 \mathrm{kgm^{-3}\,s^{-2}}$, approximating the force constant in the experiment, and using the measured values of a and $\mathscr{V}_d = \frac{4}{3}\pi(\frac{d}{2})^3$ gives a charge/volume ratio of $\rho_d \approx 1.9 \times 10^{-3}$, 3.9×10^{-3}, and $1.4 \times 10^{-2}\,\mathrm{Cm^{-3}}$ for the observed inner, middle, and outer layers, respectively. Hence, both ρ and ϕ are smallest in the outer layer and largest in the inner layer. It is straightforward to verify that, in this model, U_{tot} is minimized by ordering the layers from smallest to largest ρ_d with increasing radius (and is thus the stable configuration), given the relationship between ρ_d, ρ, and ϕ in equilibrium, despite U_e being maximized by this ordering. As an indication of the magnitudes of the forces involved, we give the x component of the external force acting on a droplet at the location $(1.0, 0, 0)$ mm: $F_x/\mathscr{V}_d = -50\,\mathrm{Nm^{-3}}$. The force acts toward the minimum in u at $(0, 0, 0)$ and is in balance with the electrostatic force acting on the droplet at $t \leq 0$.

With the addition of the acoustic forces, the droplets are confined to potential wells with larger force constants, as can be seen from the more tightly spaced contours in Figs. 2(g) and 2(h). At $(1.0, 0, 0)$ mm, the external force is $F_x/\mathscr{V}_d = 1500\,\mathrm{Nm^{-3}}$, pointing toward the potential minimum at $(2.1, 0, 0)$ mm. Since the shapes of the droplet clusters confined to these wells are highly non-spherical, a more sophisticated model of the electric field is required[36] to calculate the electrostatic forces on the droplets. Nevertheless, from our simple model, we might expect a to decrease with increasing confinement causing the droplets to coalesce, as we observe [Figs. 2(j) and 2(k)]. Most of the coalescence events occurred within the first 200 ms after the acoustic transducers were switched on and continued more infrequently over the following 3 s. The system reached a steady state after this time. Figure 2(l) shows the coalescence of two droplets with diameters 2.1 and 0.7 mm. Previous experiments[39] and numerical simulations[40] have shown that the coalescence of uncharged water droplets of this size is incomplete: satellite droplets are produced with diameter approximately half that of the smaller of the two original droplets. In contrast, we observed no such satellite droplets in this or any of the other coalescence events. The imposition of an external electric field is known to influence droplet coalescence,[40] and oppositely charged drops in an electric field above a threshold strength do not coalesce.[41] Here, the electrostatic forces between like-charged droplets appear to promote coalescence. Further experiments with higher spatial and temporal resolution are required for confirmation.

In summary, we have demonstrated a technique using a mist of charged water droplets as test particles to visualize the wells in the combined magnetic, acoustic, and gravitational potential energy of water in a sonomaglev set-up. Our experimental results agree well with a numerical model of the potential energy. In a simple spherical-parabolic model of a potential well, the spacing of the droplets in a cluster is shown to depend only on their charge and volume and on the force constant of the well. Since we have used water mist in these experiments, the results are strictly applicable only to water levitating in the magnet. However, since many diamagnetic materials have a susceptibility and density close to water, such as organic oils and plastics, results obtained from water droplets also provide a good estimate for the location of the potential wells of these materials. The acoustic wavelength λ, which governs the well size and separation, can be altered by using transducers with a different resonant frequency. For example, using 100 kHz transducers[12] would reduce the well separation by a factor of 2.5–1.7 mm.

The capacity to manipulate clusters of diamagnetically levitated drops under the action of acoustic and/or electrostatic forces has several applications. For example, previous studies have used acoustic levitators to study the evaporation rate of clusters of drops (e.g., Ref. 42). This system provides an opportunity to measure the evaporation rate of three-dimensional clusters of freely suspended drops in a quiescent system, without the complicating effects of acoustic streaming flows.[16] The self-organization of the levitated clusters can also be studied. The ability to manipulate suspended microdroplets could find applications in microfluidics and containerless chemistry. Coalescence, and so mixing, of levitated droplets or clusters of droplets can be triggered by acoustic forces, as we have demonstrated here.

The flexibility to change the forces controlling position independently of the forces required for levitation allows greater scope in manipulating material than can be achieved by acoustic or diamagnetic levitation alone. This method of experimentally visualizing the potential wells in sonomaglev will facilitate the development of more complex set-ups using more transducers, allowing for greater control over the forces acting on the levitated material in three-dimensions.

We thank Dr. B. Turnbull for the use of the high-resolution camera and S. Devlin for help with the design and printing of the PLA ring. We are grateful to the referees for helpful comments and suggestions. This work was supported by a research grant from the Leverhulme Trust (Grant No. RPG-2018-363).

AUTHOR DECLARATIONS

Conflict of Interest

The authors have no conflicts to disclose.

Author Contributions

George Hunter-Brown: Conceptualization (equal); Investigation (equal); Methodology (equal); Software (lead); Writing – original draft (equal); Writing – review & editing (equal). **Naresh Sampara:** Conceptualization (equal); Investigation (equal); Methodology (equal); Writing – original draft (equal); Writing – review & editing (equal). **Matthew M. Scase:** Conceptualization (equal); Funding acquisition (supporting); Supervision (equal); Writing – original draft (equal); Writing – review & editing (equal). **Richard J. A. Hill:** Conceptualization (equal); Funding acquisition (lead); Methodology (equal); Project administration (lead); Supervision (equal); Writing – original draft (equal); Writing – review & editing (equal).

DATA AVAILABILITY

The data that support the findings of this study are available within the article.

REFERENCES

[1]G. Hunter-Brown, N. Sampara, M. M. Scase, and R. J. A. Hill, "Sonomaglev: Combining acoustic and diamagnetic levitation," Appl. Phys. Lett. **122**, 014103 (2023).
[2]E. Beaugnon and R. Tournier, "Levitation of water and organic substances in high static magnetic fields," J. Phys. III **1**, 1423 (1991).
[3]M. V. Berry and A. K. Geim, "Of flying frogs and levitrons," Eur. J. Phys. **18**, 307 (1997).
[4]M. D. Simon and A. K. Geim, "Diamagnetic levitation: Flying frogs and floating magnets (invited)," J. Appl. Phys. **87**, 6200 (2000).
[5]Y. Ikezoe, N. Hirota, J. Nakagawa, and K. Kitazawa, "Making water levitate," Nature **393**, 749–750 (1998).
[6]T. Kimura, S. Mamada, and M. Yamato, "Separation of solid polymers by magneto-Archimedes levitation," Chem. Lett. **29**, 1294–1295 (2000).
[7]P. A. Dunne, J. Hilton, and J. M. D. Coey, "Levitation in paramagnetic liquids," J. Magn. Magn. Mater. **316**, 273 (2007).
[8]K. Bücks and H. Müller, "Über einige Beobachtungen an schwingenden Piezoquarzen und ihrem Schallfeld," Z. Phys. **84**, 75 (1933).
[9]M. A. Andrade, N. Pérez, and J. C. Adamowski, "Review of progress in acoustic levitation," Braz. J. Phys. **48**, 190–213 (2018).
[10]D. Foresti, M. Nabavi, M. Klingauf, A. Ferrari, and D. Poulikakos, "Acoustophoretic contactless transport and handling of matter in air," Proc. Natl. Acad. Sci. U. S. A. **110**, 12549–12554 (2013).
[11]T. Hoshi, Y. Ochiai, and J. Rekimoto, "Three-dimensional noncontact manipulation by opposite ultrasonic phased arrays," Jpn. J. Appl. Phys., Part 1 **53**, 07KE07 (2014).
[12]K. Melde, A. G. Mark, T. Qiu, and P. Fischer, "Holograms for acoustics," Nature **537**, 518 (2016).
[13]L. Cox, A. Croxford, B. W. Drinkwater, and A. Marzo, "Acoustic Lock: Position and orientation trapping of non-spherical sub-wavelength particles in mid-air using a single-axis acoustic levitator," Appl. Phys. Lett. **113**, 054101 (2018).
[14]E. H. Trinh and J. L. Robey, "Experimental study of streaming flows associated with ultrasonic levitators," Phys. Fluids **6**, 3567–3579 (1994).
[15]M. A. B. Andrade, N. Pérez, and J. C. Adamowski, "Experimental study of the oscillation of spheres in an acoustic levitator," J. Acoust. Soc. Am. **136**, 1518–1529 (2014).
[16]C. Lieber, S. Autenrieth, K.-Y. Schönewolf, A. Lebanoff, R. Koch, S. Smith, P. Schlinger, and H.-J. Bauer, "Application of acoustic levitation for studying convective heat and mass transfer during droplet evaporation," Int. J. Multiphase Flow **170**, 104648 (2024).
[17]A. Marzo, A. Barnes, and B. W. Drinkwater, "Tinylev: A multi-emitter single-axis acoustic levitator," Rev. Sci. Instrum. **88**, 085105 (2017).
[18]T. Kozuka, K. Yasui, T. Tuziuti, A. Towata, and Y. Iida, "Acoustic standing-wave field for manipulation in air," Jpn. J. Appl. Phys., Part 1 **47**, 4336 (2008).
[19]M. A. Andrade, N. Perez, F. Buiochi, and J. C. Adamowski, "Matrix method for acoustic levitation simulation," IEEE Trans. Ultrason., Ferroelectr., Freq. Control **58**, 1674–1683 (2011).
[20]R. Hirayama, G. Christopoulos, D. Martinez Plasencia, and S. Subramanian, "High-speed acoustic holography with arbitrary scattering objects," Sci. Adv. **8**, eabn7614 (2022).
[21]G. S. Settles, *Schlieren and Shadowgraph Techniques: Visualizing Phenomena in Transparent Media* (Springer Science & Business Media, 2001).
[22]G. S. Settles and M. J. Hargather, "A review of recent developments in Schlieren and shadowgraph techniques," Meas. Sci. Technol. **28**, 042001 (2017).
[23]B. R. Sutherland, S. B. Dalziel, G. O. Hughes, and P. Linden, "Visualization and measurement of internal waves by 'synthetic Schlieren'. Part 1. Vertically oscillating cylinder," J. Fluid Mech. **390**, 93–126 (1999).
[24]K. Bertling, J. Perchoux, T. Taimre, R. Malkin, D. Robert, A. D. Rakić, and T. Bosch, "Imaging of acoustic fields using optical feedback interferometry," Opt. Express **22**, 30346–30356 (2014).
[25]A. Kundt, "Ueber eine neue Art akustischer Staubfiguren und über die Anwendung derselben zur Bestimmung der Schallgeschwindigkeit in festen Körpern und Gasen," Ann. Phys. **203**, 497–523 (1866).
[26]A. Kundt, "III. Acoustic experiments," Philos. Mag. **35**, 41–48 (1868).
[27]L. P. Gor'kov, "On the forces acting on a small particle in an acoustic field within an ideal fluid," Dokl. Akad. Nauk SSSR **140**, 88 (1961) , [Sov. Phys.-Dokl. **6**, 773 (1962)].
[28]M. Barmatz and P. Collas, "Acoustic radiation potential on a sphere in plane, cylindrical and spherical standing wave fields," J. Acoust. Soc. Am. **77**, 928 (1985).
[29]J. F. Schenck, "The role of magnetic susceptibility in magnetic resonance imaging: MRI magnetic compatibility of the first and second kinds," Med. Phys. **23**, 815–850 (1996).
[30]R. Davis, "Equation for the volume magnetic susceptibility of moist air," Metrologia **35**, 49 (1998).
[31]W. D. Wilson, "Speed of sound in distilled water as a function of temperature and pressure," J. Acoust. Soc. Am. **31**, 1067–1072 (1959).
[32]O. Wright, "Gallery of whispers," Phys. World **25**, 31 (2012).
[33]S. Lu, X. Wang, H. Hirano, T. Tagawa, and H. Ozoe, "Water mist flow in a vertical bore of a superconducting magnet," J. Appl. Phys. **98**, 114906 (2005).
[34]F. Hecht, "New development in freefem++," J. Numer. Math. **20**, 251–266 (2012).
[35]C. Geuzaine and J.-F. Remacle, "Gmsh: A 3-D finite element mesh generator with built-in pre-and post-processing facilities," Int. J. Numer. Methods Eng. **79**, 1309–1331 (2009).
[36]Y. Kiwamoto, J. Aoki, and Y. Soga, "Potential distribution of a nonuniformly charged ellipsoid," Phys. Plasmas **11**, 4868 (2004).
[37]The expression would be exact for a continuous, spherically symmetric charge distribution, but the discrete charges produce fluctuations about this value.
[38]R. P. Feynman, R. B. Leighton, and M. Sands, *The Feynman Lectures on Physics* (Addison-Wesley, Reading, MA, 1963), Vol. 2.
[39]F. Zhang, E. Li, and S. T. Thoroddsen, "Satellite formation during coalescence of unequal size drops," Phys. Rev. Lett. **102**, 104502 (2009).
[40]M. Garzon, L. J. Gray, and J. A. Sethian, "Electrohydrodynamic coalescence of droplets using an embedded potential flow model," Phys. Rev. E **97**, 033112 (2018).
[41]W. D. Ristenpart, J. C. Bird, A. Belmonte, F. Dollar, and H. A. Stone, "Non-coalescence of oppositely charged drops," Nature **461**, 377 (2009).
[42]Y. Tian and R. E. Apfel, "A novel multiple drop levitator for the study of drop arrays," J. Aerosol Sci. **27**, 721 (1996).